Variable Switching Frequency operation of DCM Flyback Micro-inverter

Sinan Zengin and Mutlu Boztepe

Ege University, Electrical and Electronics Engineering Department, Izmir, Turkey
sinan.zengin@ege.edu.tr, mutlu.boztepe@ege.edu.tr

Abstract

Since the dedicated micro-inverters operate individual photovoltaic (PV) modules at its maximum power point, the micro-inverter topology exhibits better performance than the central and string topologies against partial shading. Among the micro-inverter topologies, discontinuous conduction mode (DCM) flyback micro-inverter is the most attractive one due to its simplest structure, easy control and potentially low cost. However it suffers from low input voltage range and high conduction loss. In this paper, a variable switching frequency control method is proposed which allows extending the input voltage range considerably. Additionally, the proposed method can decrease the total losses by 24.82% according to the simulation results.

1. Introduction

The PV modules can be connected to the utility grid using centralized, string or module type DC-AC inverters. Centralized and string type inverters require the PV modules connected in series and/or parallel. However, in serial connection, even small shading in any module can cause considerable power loss in the branch. On the other hand, module type DC-AC inverter, named as micro-inverter, is dedicated to a single PV module. Hence, each PV module can operate at its own maximum power point and the performance under partial shading condition is improved [1]. Additionally, micro-inverters have ease of manufacturing, low installation cost and modular design features, and moreover the micro-inverter topologies are more suitable for 150-300 W power levels due to these advantages [2, 3].

A PV module has single power peak on the power-to-voltage (P-V) curve under uniform irradiance condition. However, multiple power peaks may be emerged under non-uniform irradiance conditions due to the bypass diodes utilization [4, 5]. Unfortunately, another consequence of the non-uniform irradiance is the extending the PV voltage range by lowering the minimum MPP voltage.

Micro-inverters can be designed using single stage or two stage approaches. Although single stage topology has simple structure, low cost and easy control, the operating voltage range for the input port is relatively low. On the other hand, in the two stage topology, PV voltage is amplified at first stage and DC/AC inversion is realized in the second stage. Thus, it can work with wide input voltage range, but has complicated structure, high cost, difficult control and low efficiency problems [6, 7].

Single-stage micro-inverter topologies are well studied in literature [6–9] and DCM flyback micro-inverter based topologies are the most attractive one due to simple control. Unfortunately as the input voltage range increases, the efficiency of the micro-inverter decreases due to increased conduction loss.

In this paper, a variable switching frequency control of DCM flyback micro-inverter is proposed which allows extending the input voltage range without increasing the conduction loss. In section 2 the maximum voltage range for a PV module is analyzed. In section 3 and 4, design of the flyback micro-inverter are presented for constant and variable switching frequency operation, respectively. Simulation results are given in the section 5 and the conclusion is drawn in the section 6.

2. PV Module Characteristics

The electrical equivalent circuit is commonly used model for characterizing the solar cells [10]. By using the equivalent circuit, the terminal current I of a PV module that consist of N_s solar cells connected in series can be expressed as;

$$I = I_{ph} - I_s\left(e^{\frac{q(V+IR_s)}{aN_skT}} - 1\right) - \frac{V+IR_s}{R_p} \qquad (1)$$

where I_{ph} is the photon current, I_s is diode saturation current, V is PV module terminal voltage, q is the electric charge constant $(1.6\times10^{-19}C)$, k is the Boltzmann constant $(1.38\times10^{-23}\,\mathrm{J/K})$ and a is diode ideality factor. R_s and R_p are series and shunt resistances, respectively. Additionally, the parallel resistance R_p is very large in modern solar cells, and can be neglected for simplifying the calculations [11]. The model parameters at STC (Standard test conditions, 1000 W/m^2, 25°C, A.M. 1.5) for OST-80 polycrystalline PV module which is manufactured by Orjin Solar Technology Ltd. in Turkey are listed in Table 1. OST-80 PV module, which consists of 36 cells connected in series and two bypass diodes per module, is used in the all analysis in the paper.

Table 1. OST-80 model parameters at STC

Parameter	Value
Maximum Power, P_{mp} [W]	80
Open circuit voltage, V_{oc} [V]	22
Short circuit current, I_{sc} [A]	4.9
Maximum power voltage, V_{mp} [V]	18
Maximum power current, I_{mp} [A]	4.5
Photon current, I_{ph} [A]	4.9
Diode saturation current, I_S [A]	$5.8273\text{x}10^{-7}$
Diode ideality factor, a	1.49195
Series resistance, R_S, [Ohm]	0.1206
Number of cell, N_s	36
Number of bypass diodes	2

2.1. Uniform Irradiation Condition

Under uniform irradiation condition, the current-voltage (I-V) and the power-voltage (P-V) curves of the OST-80 PV module are shown together in the Fig.1. In this condition, there is only one power peak in the P-V curve which is called as maximum power point MPP. However the MPP point depends on the solar irradiation and cell temperature strongly. The MPP loci on the P-V curve for various irradiance and temperature values are depicted in the Fig. 2. It can be seen from this figure that, as the temperature increases, the MPP voltage decreases. On the other hand, the irradiance strongly affects the power of the PV module.

2.2. Non-uniform Irradiation Condition

Under non-uniform irradiation condition the P-V curve has two power peaks (or two local MPP's, LMPP) due to the bypass diode conduction. However, only one of them is the globally maximum (GMPP) according to the shading pattern. For

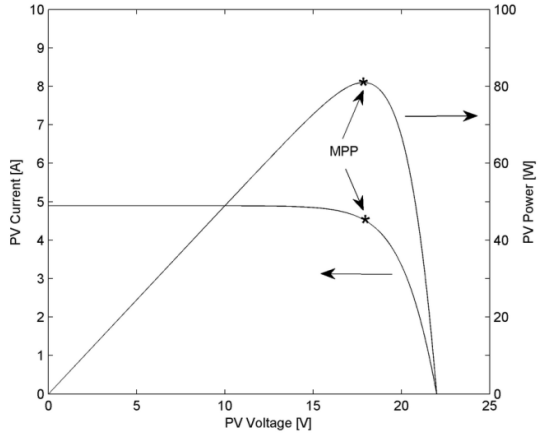

Fig. 1. Characteristic curves of OST-80 under uniform irradiation at STC

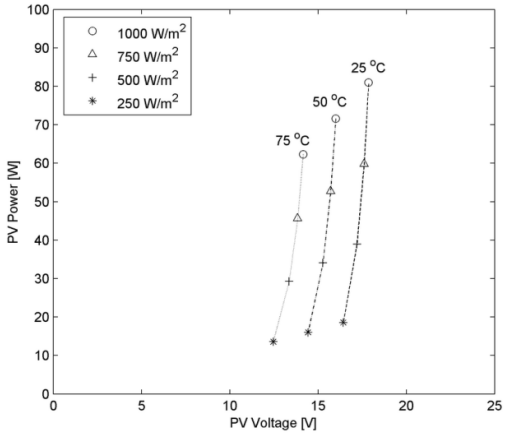

Fig. 2. MPP loci for various irradiances and temperatures

example, the P-V curve of OST-80 under global irradiation of 1000 W/m^2 is shown in Fig. 3 for three different shading cases; such as (1) no shading, (2) half of the module (18 cells) is shaded with 600 W/m^2 and (3) half of the module (18 cells) is shaded with 300 W/m^2. The 18 cells are belongs to one bypass diode in the PV module. It is understood from the Fig. 3 that, while the shaded irradiance is higher than 500 W/m^2, which corresponds to the 50% irradiance of STC, the first LMPP point is always the global MPP. In other cases, the second local peak, which has lower voltage than the first, becomes global MPP.

The minimum input voltage and the maximum input power are key parameters for designing a flyback micro-inverter. Therefore in order to determine the key parameters, the LMPP points for the PV module are calculated for four different irradiance cases and three different cell temperatures as shown in Fig. 4. In the calculation of 2nd LMPPs, it is assumed that while one half of the PV module is totally shaded (with 0 W/m^2)

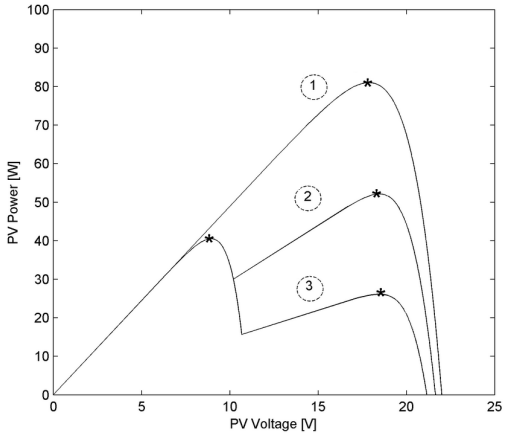

Fig. 3. P-V curves for three different shading scenarios

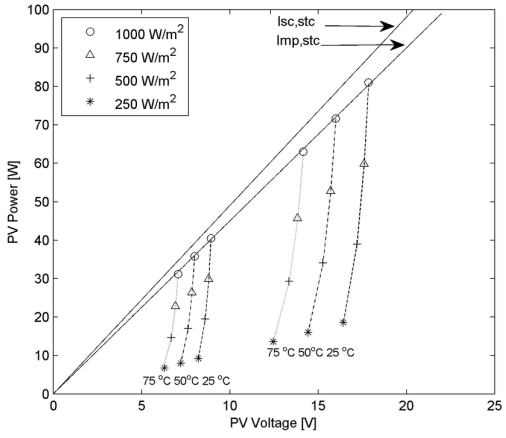

Fig. 4. PV module LMPPs for different environmental conditions

meanwhile the irradiance varies for the other half. From the Fig. 4, a linear relationship between the maximum PV power and the PV voltage can be defined as depicted by a straight line in the figure. Therefore, all the operating points of PV module must be below than this straight line. The slope of the line is I_{mp}, but it

depends on the environmental conditions apparently, hence conservatively it is assumed as I_{sc} at STC.

3. Analysis of DCM Flyback Micro-inverter

Fig. 5 shows the principal schematics of the conventional DCM flyback micro-inverter topology. In this topology, there are three main switches; S1, S2 and S3. Briefly, the S1 is modulated at high frequency to obtain sinusoidal wave shape on the output current, whereas the S2 and S3 are operated at the grid frequency in order to select the polarity of the grid cycle for proper operation.

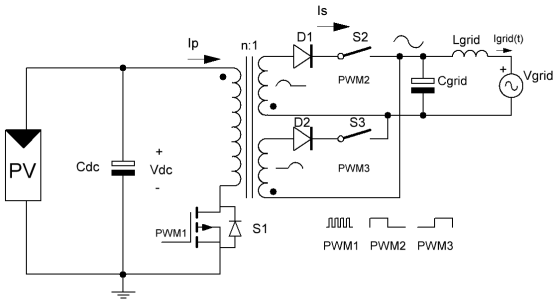

Fig. 5. Principal schematic of DCM flyback micro-inverter

When S1 is turned on for duration of t_{on}, the certain amount of energy is stored in magnetizing inductance L_m. After that the S1 is turned off for duration of t_{off}, and then the stored energy is transferred to the utility grid through S2-D1 or S3-D2 switches according to the grid cycle. For DCM operation, the total time ($=t_{on}+t_{off}$) has to be shorter than the switching period of T_s of S1. Hence the maximum duty ratio must obey the following inequality;

$$D_m \le \frac{1}{1+(V_{dc}/nV_{grid,\max})} \tag{2}$$

where n is flyback transformer turns ratio, $V_{grid,max}$ is the peak voltage of the utility grid, V_{dc} is the input DC voltage.

The turns ratio n can be determined by using the breakdown voltage V_{br} of a specified mosfet and clamp voltage V_{clamp} as follows,

$$V_{br} = V_{clamp} + V_{dc} \tag{3}$$

where V_{clamp} can be selected between $2nV_{grid,max} < V_{clamp} < 2.5nV_{grid,max}$ [12]. The S1 is modulated so as to make the output current rectified sinusoidal wave shape. Therefore the conduction time of S1 can be expressed as below;

$$T_{on}(t) = |D_m T_s \sin(\omega t)| \tag{4}$$

where ω is the grid frequency in rad/sec. Due to DCM operation, the peak current of S1 can be calculated by multiplying (4) with the turn-on slope of magnetizing current.

$$I_{S1,peak}(\mathrm{t}) = \frac{V_{dc}}{L_m}|D_m T_s \sin(\omega t)| \tag{5}$$

Averaging over the switching period is an effective method to remove the high frequency switching ripples, as given below [13].

$$< x(t) >_{T_s} = \frac{1}{T_s}\int_{t}^{t+T_s} x(t)\,dt \tag{6}$$

Therefore, the averaging the $I_{S1,peak}$ over the switching period T_s yields;

$$I_{S1}(\mathrm{t}) = \frac{V_{dc}}{2L_m} D_m{}^2 T_s \,|\, sin^2(\omega t)\,| \tag{7}$$

The input power P_{in}, can be calculated by multiplying (7) with V_{dc},

$$P_{in}(\mathrm{t}) = \frac{V_{dc}{}^2}{2L_m} D_m{}^2 T_s \,|\, sin^2(\omega t)\,| \tag{8}$$

The average input power $P_{in,avg}$ can then be calculated by time averaging of (8).

$$P_{in,avg} = \frac{1}{T}\int_0^T P_{in}(\mathrm{t})\mathrm{dt} = \frac{1}{4L_m f_s} V_{dc}^2 D_m{}^2 \tag{9}$$

where the T is grid period and f_s is switching frequency of S1.

In order to determine the parameters L_m, n, D_m and f_s, the conventional constant switching frequency design method of DCM flyback micro-inverter uses the minimum input voltage that is nearly 7 Volts for OST-80 PV module. The micro-inverter parameters determined for this minimum voltage are listed in Table 2. The flyback micro-inverter output power with respects to the input PV voltage is also drawn in Fig. 6. The intersection point A is the key operating point for the conventional constant switching frequency design procedure.

Table 2. The parameters for DCM flyback micro-inverter with constant switching frequency operation

Parameter	Value
Maximum Duty, D_m @ 7V	0.8698
Switching Frequency, f_s	100 kHz
Turn Ratio, n	0.167
Maximum Grid Voltage, $V_{grid,max}$	325 V ± 15%
Magnetizing Inductance, L_m	2.7018 uH

However, as can be seen from the Fig. 6, while the micro-inverter power is well-balanced with the PV power at low voltage values, e.g. point A, there is substantial difference between them at high voltage levels. As a result, the conduction loss in the switch S1 and in the transformer winding increases very much at high PV voltage levels. The conduction loss is proportional to the square of the rms current and it can be calculated as follows [14],

$$I_{p,rms} = \sqrt{\frac{4}{9\pi}\frac{V_{dc}^2 d_p{}^3}{L_m{}^2 f_s{}^2}} \tag{10}$$

where d_p is the actual duty ratio ($d_p<D_m$). By combining (9) and (10), $I_{p,rms}$ can be written as follows;

$$I_{p,rms} = \sqrt{\frac{32}{9\pi} \frac{P_{in,avg}^{3/2}}{V_{dc}(L_m f_s)^{1/2}}} \quad (11)$$

The plot of the maximum primary rms current with respects to the PV voltage for conventional constant switching frequency DCM flyback micro-inverter is shown in Fig. 9. As mentioned before, there is a considerable increment in the rms current, approximately 21%, over the input voltage range. The increase in the rms current not only causes to increase the conduction loss, but also may results in using higher magnetic core which increases the weight and the volume of the converter. The proposed variable switching frequency control described in the following section in detail which can solve this problem, and reduce the rms current at high voltage levels effectively.

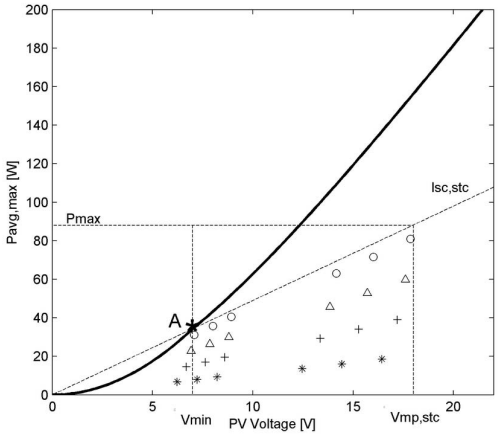

Fig. 6. Conventional Flyback DCM micro-inverter power-voltage characteristic

4. Variable Switching Frequency Control Method

In the section 2, a straight line whose slope is equal to $I_{sc,stc}$ is defined as a border for operational points of the PV module as shown in Fig. 4. This straight line can be represented by,

$$P_{pv} = V_{dc} I_{sc,stc} \quad (12)$$

On the other hand, the input power of the flyback micro-inverter is defined by (9). In the proposed method, the proper switching frequency is calculated by equating these equations, P_{pv}=$P_{in,avg}$. Thus, the switching frequency f_s is found by combining (9) and (12),

$$f_s = KV_{dc} \quad (13)$$

where the K is constant, and defined as;

$$K = \frac{D_m^{\,2}}{4L_m I_{sc,stc}} \quad (14)$$

The inverter parameters used in the calculations for variable switching frequency operation are listed in Table 3.

Table 3. The parameters for DCM flyback micro-inverter for variable switching frequency operation

Parameter	Value
Maximum Duty, D_m @ 18V	0.7224
Switching Frequency, f_s	100 kHz
Turn Ratio, n	0.167
Maximum Grid voltage, $V_{grid,max}$	325 V ± 15%
Magnetizing Inductance, L_m	4.792 uH

The Fig. 8 shows the power-to-voltage curves for the micro-inverter and PV module simultaneously. It should be noted that, the intersection point B is the key operating point for the variable switching frequency design procedure. The operating point can be shifted down to the point A by decreasing the switching frequency from 100 kHz to 40 kHz without increasing the rms current of the switch.

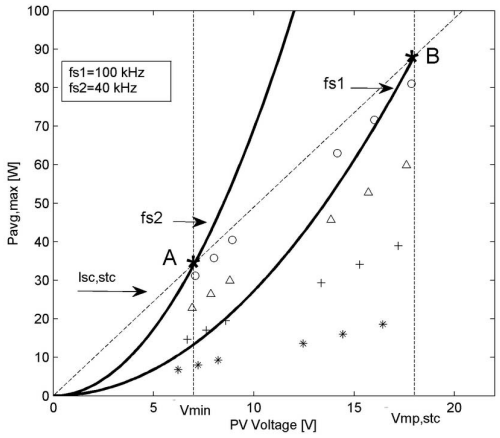

Fig. 7. Power-to-voltage curves for proposed method

5. Simulation Results

For validating the proposed method, the simulation of DCM flyback micro-inverter was realized by using LTSPICE®. Fig. 8 shows the simulated circuit diagram with values of proposed method as listed in Table 4. Leakage inductance, copper loss and core losses of the transformer are ignored in the simulation.

Fig. 9 shows the calculated and simulated values of primary rms currents with respects to the PV voltage for conventional and proposed methods. According to the simulation results, the proposed method decreases the primary rms current 13.16% at nominal power of 80 W. Moreover, the switching losses is also decreased by proposed method since the peak current of the mosfet switch S1 ($I_{s1,peak}$) is reduced. Total losses, which includes switching and conduction losses of the all mosfets and diodes in the circuits, is decreased by %24.82 at nominal power by making the switching frequency variable.

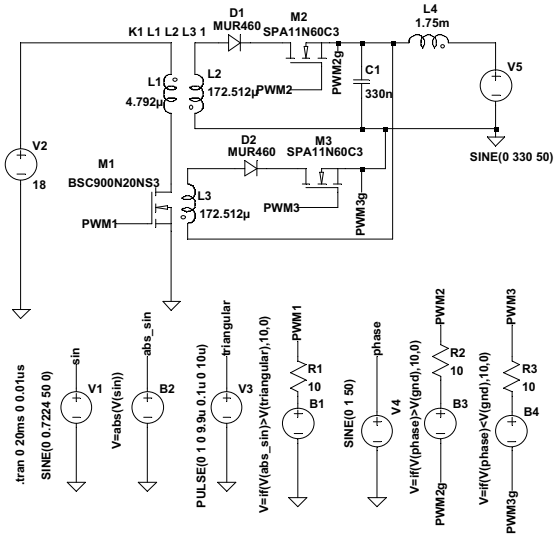

Fig. 8. The circuit diagram of the simulated DCM flyback micro-inverter.

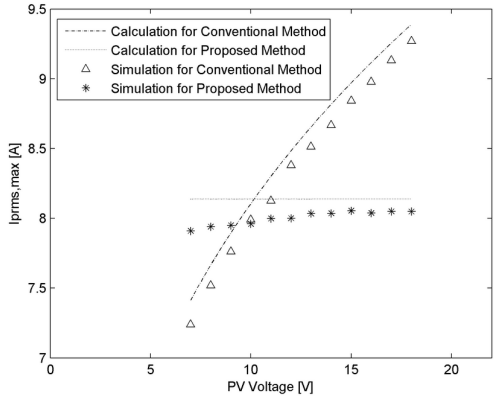

Fig. 9. Primary rms currents for proposed and conventional methods

Table 4. The parameters for DCM flyback micro-inverter in simulations

Parameter	Value
Output Filter (L_{grid}, C_{grid})	1.75 mH/330 nF
S1 Mosfet	BSC900N20NS3
S2-S3 Mosfets	SPA11N60C3
D2-D3 Diodes	MUR460

6. Conclusion

The constant switching frequency operation of DCM flyback micro-inverter suffers from low input voltage range and high conduction loss. In this paper, a variable switching frequency control method is proposed which allows extending the input voltage range significantly. Additionally, the proposed method reduces the rms current considerably, and in turn, the total losses (except transformer losses) in the micro-inverter are decreased by 24.82%.

7. References

[1] S. V Dhople, J. L. Ehlmann, A. Davoudi, and P. L. Chapman, "Multiple-input boost converter to minimize power losses due to partial shading in photovoltaic modules," in Energy Conversion Congress and Exposition ECCE 2010 IEEE, 2010, pp. 2633–2636.

[2] H. Hu, S. Harb, N. Kutkut, I. Batarseh, and Z. J. Shen, "Power Decoupling Techniques for Micro-inverters in PV Systems-a Review," in Energy Conversion Congress and Exposition (ECCE), 2010 IEEE, 2010, pp. 3235–3240.

[3] J.-M. Kwon, B.-H. Kwon, and K.-H. Nam, "High-efficiency module-integrated photovoltaic power conditioning system," IET Power Electronics, vol. 2, no. 4, pp. 410–420, 2009.

[4] E. Karatepe, Syafaruddin, and T. Hiyama, "Simple and high-efficiency photovoltaic system under non-uniform operating conditions," IET Renewable Power Generation, vol. 4, no. 4, pp. 354–368, 2010.

[5] E. V Paraskevadaki and S. A. Papathanassiou, "Evaluation of MPP Voltage and Power of mc-Si PV Modules in Partial Shading Conditions," IEEE Trans. on Energy Conversion, vol. 26, no. 3, pp. 923–932, 2011.

[6] Y. Xue, L. Chang, and S. B. Kjær, "Topologies of Single-Phase Inverters for Small Distributed Power Generators : An Overview," IEEE Tran. on Power Electronics, vol. 19, no. 5, pp. 1305–1314, 2004.

[7] Q. Li and P. Wolfs, "A Review of the Single Phase Photovoltaic Module Integrated Converter Topologies With Three Different DC Link Configurations," IEEE Tran. on Power Electronics, vol. 23, no. 3, pp. 1320–1333, 2008.

[8] S. B. Kjaer, J. K. Pedersen, and F. Blaabjerg, "A Review of Single-Phase Grid-Connected Inverters for Photovoltaic Modules," IEEE Trans. on Industry Applications, vol. 41, no. 5, pp. 1292–1306, 2005.

[9] S. Zengin, F. Deveci, and M. Boztepe, "Decoupling Capacitor Selection in DCM Flyback PV Microinverters Considering Harmonic Distortion," IEEE Transactions on Power Electronics, vol. 28, no. 2, pp. 816–825, Feb. 2013.

[10] E. Karatepe, M. Boztepe, and M. Colak, "Neural network based solar cell model," Energy Conversion and Management, vol. 47, no. 9–10, pp. 1159–1178, Jun. 2006.

[11] J. A. Duffie and W. A. Beckman, Solar Engineering and Thermal Processes. 1991, p. 919.

[12] F. Semiconductor, "Application Note AN-4147 Design Guidelines for RCD Snubber of Flyback Converters." 2006.

[13] R. W. Erickson and D. Maksimovic, Fundamentals of Power Electronics. Kluwer Academic Publishers, 2001, p. 883.

[14] A. C. Nanakos, E. C. Tatakis and N. P. Papanikolaou "A Weighted-Efficiency-Oriented Design Methodology of Flyback Inverter for AC Photovoltaic Modules," IEEE Tran. on Power Electronics, vol. 27, no. 7, pp. 3221–3233, 2012.